Journal of Pharmaceutical Innovation (2025) 20:181
https://doi.org/10.1007/s12247-025-10104-6

RESEARCH

Development and Evaluation of a PH-Responsive Bovine Serum Albumin-Functionalized Layered Double Hydroxide Nanocarrier for Targeted Therapy of Ovarian Cancer

Mervat Shafik Ibrahim[1] · Nihal Mohamed Elmahdy Elsayyad[1] · Shereen H. Noshi[1]

Received: 24 May 2025 / Accepted: 3 September 2025

Abstract

Purpose Ovarian cancer accounts for 4.7% of cancer-related deaths in women, with paclitaxel (PAC) being an effective treatment option. However, poor water solubility and inefficient release within the tumor microenvironment limit its clinical use. This study aims to optimize a novel PAC pH-sensitive nanocarrier system based on layered double hydroxide (LDH) functionalized with bovine serum albumin (BSA) to enhance its delivery and release.

Methods A response surface D-optimal design was utilized to optimize the formulation of BSA-d-LDH-PAC nanoparticles, considering particle size (PS), drug entrapment efficiency (EE%), and zeta potential (ZP). The optimized formulation (F3) was characterized using structural and physicochemical analyses, and in vitro drug release studies were conducted at different pH levels. Additionally, cytotoxicity studies were performed to evaluate the therapeutic potential of the developed system.

Results The optimized formulation (F3) incorporated 16 mg/mL BSA, 0.5 mg PAC, and delaminated layered double hydroxide (d-LDH), yielding nanoparticles with a brucite-like structure, a diameter of 95 nm, a ZP of -27 mV, and an EE% of 51%. Molecular modeling and FTIR analysis confirmed the layered LDH structure and successful integration of BSA and PAC via hydrogen bonding, contributing to high drug loading and entrapment efficiency. The less ordered particle arrangement enhanced PAC aqueous solubility and facilitated rapid release, with 90% of the drug released at pH 5.5 within 5 h. Cytotoxicity studies demonstrated the superior anticancer activity of BSA-d-LDH-PAC compared to free PAC suspension.

Conclusion BSA-functionalized LDH nanoparticles provide an efficient, pH-responsive delivery system for PAC, improving solubility, controlled release, and cytotoxic efficacy. These findings emphasize the future promise of this nanocarrier system for enhanced ovarian cancer treatment and broader applications in targeted drug delivery.

Keywords Ovarian cancer; paclitaxel · Layered double hydroxide (LDH) · PH-sensitive nanocarriers · Targeted cancer therapy

Introduction

Ovarian cancer remains a major global health challenge, ranking as the eighth most common malignancy among women and accounting for approximately 4.7% of cancer-related deaths worldwide [1]. Despite advances in treatment, chemotherapy continues to be the primary therapeutic approach, yet severe systemic side effects often compromise its effectiveness. Traditional cytotoxic agents, such as paclitaxel (PAC), indiscriminately target rapidly dividing cells, leading to collateral damage in healthy tissues and resulting in complications like myelosuppression, mucositis, and alopecia. These adverse effects not only diminish patients'

✉ Nihal Mohamed Elmahdy Elsayyad
nmahdy@msa.edu.eg

Mervat Shafik Ibrahim
mshafik@msa.edu.eg

Shereen H. Noshi
shamdi@msa.edu.eg

[1] Department of Pharmaceutics and Industrial Pharmacy, Faculty of Pharmacy, October University for Modern Sciences and Arts (MSA), Giza, Egypt

Published online: 22 September 2025

quality of life but also hinder treatment adherence and outcomes [2].

Paclitaxel (PAC) is a potent chemotherapeutic agent with proven efficacy against a range of cancers, including ovarian, breast, and lung malignancies [3–5]. Its mechanism of action involves stabilizing microtubules and inducing apoptosis during the G2/M phase of the cell cycle. However, PAC's clinical utility is significantly limited by its poor aqueous solubility (0.1 μg/mL) and low bioavailability, which necessitate the use of solubilizing agents such as Cremophor EL (CrEL) in commercial formulations like Taxol. Unfortunately, CrEL has been associated with hypersensitivity reactions, altered lipid metabolism, and neurotoxicity, prompting the search for safer and more effective delivery systems [6–8].

Nanomedicine has emerged as a promising solution to the limitations of conventional chemotherapy, offering enhanced drug solubility, improved pharmacokinetics, and targeted delivery to tumor tissues while minimizing systemic toxicity [9, 10]. Over the past decade, a wide array of nanocarrier platforms has been developed to address the challenges associated with hydrophobic drugs like paclitaxel (PAC). These include albumin-bound nanoparticles (e.g., Abraxane®), polymeric micelles (e.g., Cynviloq®, Nanoxel®, Paclical®), liposomes (e.g., Lipusu®), and polymeric lipidic nanoparticles, many of which have progressed to clinical trials or received regulatory approval [9, 10]. These systems have demonstrated improved drug loading, prolonged circulation time, and enhanced accumulation in tumor tissues via the enhanced permeability and retention (EPR) effect. However, despite these advancements, several limitations persist, including premature drug leakage, complex manufacturing processes, and limited control over drug release kinetics.

To overcome these challenges, researchers have increasingly turned to inorganic nanocarriers, which offer unique physicochemical properties that can be tailored for more effective drug delivery. Among these, layered double hydroxides (LDHs) have gained significant attention due to their high surface area, tunable composition, and anion exchange capacity, which facilitate efficient drug encapsulation and controlled release [11, 12]. Furthermore, LDHs exhibit superior chemical stability in various solvents compared to many polymeric carriers, making them attractive candidates for long-term drug storage and formulation development [13]LDHs are composed of positively charged metal hydroxide layers intercalated with exchangeable anions, allowing for the incorporation of negatively charged drug molecules such as PAC through electrostatic interactions [14–21]. One of the most compelling features of LDHs is their pH-responsive behavior: under physiological conditions (pH 7.4), LDHs exhibit sustained drug release, while in the acidic tumor microenvironment (pH 6.5–7.2), partial dissolution of the LDH matrix triggers a burst release of the drug which enhances therapeutic efficacy at the tumor site while minimizing exposure to healthy tissues, thereby reducing systemic toxicity [22].

Their biocompatibility and ability to be functionalized with targeting ligands or stabilizing agents further expand their versatility in cancer therapy. Recent studies have demonstrated the successful incorporation of PAC into LDH-based composites, such as ZnAl-LDH combined with cobalt ferrite and N-graphene quantum dots (N-GQDs), which showed high drug loading capacity and pH-sensitive release profiles [23]. These findings underscore the potential of LDHs as next-generation nanocarriers capable of delivering therapeutic doses of PAC directly to tumor cells while minimizing off-target effects.

In order to improve the efficacy of LDH-based carriers, the incorporation of biomolecules, including bovine serum albumin (BSA), has proven to be an effective approach. Bovine serum albumin (BSA) is a natural protein and is known for its biocompatibility, remarkable stability, and strong binding capacity for various molecules. These characteristics position it as an excellent choice for the modification of nanoparticle surfaces. The capacity to engage with Gp60 receptors present on endothelial cells enhances the process of transcytosis, thereby promoting the accumulation of drugs within tumor tissues [8]. Furthermore, BSA can stabilize nanoparticles by means of electrostatic and steric interactions, which effectively inhibit aggregation and extend their circulation time. The functionalization of layered double hydroxides (LDHs) with bovine serum albumin (BSA) significantly enhances their ability to target specific sites. It improves their physicochemical stability, thereby rendering them more appropriate for clinical applications [8].

In this study, a novel pH-responsive, BSA-functionalized LDH nanocarrier was developed for the targeted delivery of PAC. The LDH was synthesized using magnesium and aluminum nitrates and functionalized with native BSA to enhance particle stability and tumor targeting. A D-optimal design approach is used to optimize the formulation due to its flexibility and efficiency [24]. The optimized formula was selected based on a desirability index that incorporated particle size, drug entrapment efficiency, and zeta potential. Molecular modeling was conducted to elucidate the interaction mechanisms between PAC, BSA, and the LDH matrix, providing insight into the structural basis of drug loading. The optimized formulation was then subjected to comprehensive characterization, including pH-dependent drug release studies, physicochemical analysis, and in vitro cytotoxicity assays using the KF-28 ovarian cancer cell line. This work aims to demonstrate the potential of BSA-functionalized LDHs as a next-generation nanocarrier system for improving PAC delivery and therapeutic efficacy in ovarian cancer treatment.

Experimental

Materials

Paclitaxel (PAC) was obtained as a free sample from Fresenius Kabi (Egypt). Magnesium nitrate hexahydrate (MgNO3·6H2O), aluminium nitrate nonahydrate (AlNO3·9H2O), and bovine serum albumin (BSA) were purchased from Sigma-Aldrich (USA). Disodium hydrogen phosphate and potassium dihydrogen phosphate were obtained from El-Nasr Pharmaceutical Chemicals Co. (Egypt). Sodium hydroxide was purchased from PioChem (Egypt). Methanol was obtained from Biochem Chemicals (Egypt). All other solvents were of analytical grade and used as received.

Preparation of Layered Double Hydroxides (LDHs)

The coprecipitation process was used to synthesize double-layered hydroxide nanoparticles. An amount of 2.25 g of $AlNO_3$ and 4.16 g of $MgNO_3$ were weighed precisely and dissolved in 400 mL of deionized water. The nitrates solution was kept under vigorous stirring and titrated with 1% NaOH solution until the pH reached 9.5 and a white precipitate developed. The yield was subjected to a post-precipitation hydrothermal treatment at 150 C° for 16 h to improve the particle size and crystallinity. The produced particles labeled as bulk-LDH were then filtered, oven dried, transferred, and divided into two portions. Following synthesis, the surface area of the LDH nanocarriers was increased using two post-synthesis treatments: delamination and calcination. In delamination, the particles were dispersed in methanol and sonicated to promote exfoliation of the LDH layers, resulting in delaminated LDH (d-LDH). The nanocarriers were subjected to a furnace treatment at 450 °C for 9 h for calcination. These calcined nanocarriers were designated as c-LDH. The resulting nanocarriers were stored in a sealed container for future use [25–28].

Paclitaxel Loading on LDH (LDH-PAC)

Three different concentrations of PAC (0.5, 1, and 8 mg) were loaded on LDH to determine the particle entrapment efficiency (EE%). The drug was first dissolved in an appropriate volume of methanol, and 16 mg of d-LDH or c-LDH and 18 mL of distilled water were added. The mixture was left in an incubator (J.P Selecta ZHWY-2102 C, Spain) for 48 h. at 40 ◦C to evaporate the methanol. The samples were then centrifuged using a Laborzentrifugen, 2k15, Sigma, Germany centrifuge set at a speed of 15,000 rpm for 30 min. The precipitate was washed twice with distilled water and freeze-dried using a Christ freeze-drier (Alpha 2.4 LD plus, Germany) at − 20 °C and pressure 0.02 mbar for 24 h [25].

Functionalization of PAC-LDH with Bovine Serum Albumin (BSA)

A range of BSA solutions was prepared in distilled water. The freeze-dried PAC-LDH samples were redispersed in distilled water, and the BSA solutions were added dropwise to the LDH dispersed particles under vigorous stirring. The BSA concentration in the mixture was adjusted to be 1, 2, 4, 8, and 16 mg/ml. The mixture was left for 30 min on a magnetic stirrer (MMS-3000, Biosan LTD, UK) to form BSA functionalized PAC-LDH (BSA-LDH-PAC) and then centrifuged and sent to freeze drying to be stored in powder form in a cool, dry place [29].

Design of Experiments for Sample Preparation and Characterization

To investigate the influence of formulation variables on BSA-LDH-PAC properties and their optimization through D-optimal design using Design-Expert® 12.0.3.0 software (Stat-Ease Inc., USA). In this design, three independent factors were evaluated, namely (A) the PAC concentration, (B) the BSA concentration, and (C) the post-synthesis treatment. The dependent variables were particle size (PS) (R1), (ZP) (R2), and EE% (R3). Paclitaxel concentration varied across three levels (0.5, 1, and 8 mg), while BSA concentration was tested at five levels (0, 4, 8, 10, and 16 mg). The type of LDH was investigated at two levels (d-LDH and c-LDH). As outlined in Table 1, a total of fifteen experimental combinations were evaluated. Detailed information about the components and their corresponding levels can be found in the supplementary section (Table S1). Moreover, the best-fitted models for both R1, R2, and R3 were selected based on the lowest model p-value (significant), highest R2 value, highest lack of fit p-value (non-significant), and where the difference between the predicted R2 and the adjusted R^2 is in reasonable agreement (less than 0.2). Based on the desirability approach, numerical optimization was carried out by keeping the PS between 0 and 100 nm, maximizing EE%, and the magnitude of ZP. All factor weights were considered equally important and thus were set to 1/3. The optimized formula achieved the highest desirability index and was chosen for future studies.

The optimized formulation was replicated and evaluated by comparing experimental and predicted values for PS and EE%. A low percentage bias confirmed the model's validity. Further characterization of the optimized formulation included drug release studies, physicochemical properties, and in vitro cytotoxicity assessment.

Characterization of BSA-LDH-PAC

Measurement of Particle Size (PS) and zeta-potential (ZP) Particle size (PS) and zeta potential (ZP) were

Table 1 The independent variables, namely PAC, PSA concentration, synthesis method, and measured responses of LDH particles (particle size, zeta potential, and entrapment efficiency) according to D-optimal design ($n=3$)

	Factor 1	Factor 2	Factor 3	Response 1	Response 2	Response 3
Run	**A: [PAC (mg)]**	**B: [BSA (mg)]**	**C: Synthesis**	**PS (nm)**	**ZP (mV)**	**EE%**
1	0.5	0	c-LDH	101.3 ± 1.2	26.7 ± 0.5	2.4 ± 0.3
2	8	16	c-LDH	121.1 ± 1.5	−27.1 ± 0.7	1.8 ± 0.2
3	0.5	16	d-LDH	95.2 ± 1.0	−27.0 ± 0.6	51.2 ± 0.5
4	8	8	d-LDH	331.2 ± 2.0	−17.2 ± 0.8	9.7 ± 0.4
5	0.5	8	c-LDH	349.4 ± 1.8	−19.1 ± 0.6	3.2 ± 0.3
6	1	16	c-LDH	120.6 ± 1.1	−27.2 ± 0.7	2.7 ± 0.2
7	1	4	d-LDH	339.5 ± 1.9	−15.3 ± 0.5	30.0 ± 0.3
8	8	8	c-LDH	343.8 ± 1.7	−17.1 ± 0.6	3.1 ± 0.2
9	8	0	c-LDH	102.9 ± 1.3	26.8 ± 0.4	2.6 ± 0.3
10	8	16	d-LDH	93.7 ± 1.2	−27.2 ± 0.5	1.9 ± 0.2
11	8	0	d-LDH	90.5 ± 1.0	27.1 ± 0.6	3.3 ± 0.3
12	1	16	c-LDH	121.8 ± 1.4	−27.2 ± 0.7	1.5 ± 0.2
13	1	10	d-LDH	299.4 ± 1.6	−20.2 ± 0.5	21.0 ± 0.4
14	0.5	16	d-LDH	96.7 ± 1.3	−27.1 ± 0.6	3.9 ± 0.3
15	8	16	c-LDH	119.2 ± 1.5	−26.8 ± 0.5	2.8 ± 0.3

determined using a Malvern Zetasizer Nano-ZS (Nano-ZS, UK). Samples were diluted appropriately with distilled water before analysis. Measurements were conducted at ambient temperature in disposable zeta potential cuvettes [30, 31].

PAC Entrapment Efficiency in BSA-LDH-PAC (EE%) Drug entrapment efficiency (EE%) was determined using high-performance liquid chromatography (HPLC-UV) with an Agilent 1100 series system (Agilent Technologies, Diegem, BE). A reverse-phase CC 125/4 Nucleod UR 100-5 C18 column was employed under the following conditions: column temperature 25 °C, flow rate 1.0 mL/min, injection volume 50 µL, and detection wavelength 227 nm. A known amount of BSA-LDH-PAC was dissolved in acetonitrile, shaken for 30 min, and filtered. The paclitaxel content was determined using HPLC, and EE% was calculated as:

$$EE\ (\%) = \frac{D_i}{D_t} \times\ 100 \tag{1}$$

Where Di is the amount of drug entrapped in the particles, and Dt is the total amount of drug added [32, 33].

Fourier Transform Infrared Spectroscopy (FTIR) FTIR spectroscopy was employed to corroborate the molecular modelling findings. Powder samples of plain LDH, PAC, BSA, and the optimized BSA-LDH-PAC formulation were mixed with KBr and pressed into thin films. Spectra were collected using a Shimadzu IR Affinity spectrometer within the 0–4000 cm^{-1} range at a resolution of 4 cm^{-1} [34, 35].

Molecular Modelling The paclitaxel (PAC) loading mechanism onto the LDH surface and BSA functionalization were computationally investigated using Maestro software (Maestro version 13.5.128, Schrodinger, USA). An LDH structure, obtained from the Materials Project, was processed into a 5 × 5 × 5 repeated crystal structure using Avogadro software (an open-source molecular builder and visualization tool), Version 1. XX. http://avogadro.cc/) [36, 37] BSA and PAC structures were sourced from the RCSB Protein Data Bank (https://www.rcsb.org/structure/4f5s, accessed 15/6/2024) and PubChem (accessed 15/6/2024), respectively. After importing these structures into Maestro and performing energy minimization, intramolecular interactions between LDH layers, LDH and PAC, and LDH and BSA were determined [38].

Transmission Electron Microscopy (TEM) The morphology of the optimized BSA-LDH-PAC formulation was examined using a JEM-2100 TEM microscope (Jeol, Japan). An aqueous dispersion of the formulation was applied to a carbon-coated copper grid and allowed to dry before imaging [39, 40].

Differential Scanning Calorimetry (DSC) Differential scanning calorimetry (DSC) was performed on freeze-dried LDH and the optimized formulation, as well as on the powder form of PAC and BSA. Samples were accurately weighed and sealed in standard aluminium pans. Thermograms were recorded from 30 to 300 °C under Liquid nitrogen at a heating rate of 5 °C/min [24].

X-ray Diffraction (XRD) X-ray diffraction (XRD) patterns were obtained for freeze-dried LDH and the optimized formulation, as well as for PAC and BSA powders using a Bruker D8 diffractometer. Diffractograms were collected

from 4° to 90° in 2θ using a Ni-filtered Cu Kα X-ray source operated at 40 kV and 40 mA [41].

In Vitro Drug Studies Drug release kinetics were evaluated using a Franz diffusion cell system. Freeze-dried BSA-LDH-PAC, drug powder reconstituted in phosphate buffers at pH 7.4 (simulating extracellular fluids and blood) and pH 5.5 (simulating cancer tissue) to achieve a PAC concentration of 5 mg/mL. Samples were enclosed in dialysis bags (Dialysis tubing cellulose membrane, Sigma Co., USA; Molecular weight cutoff 12,000–14,000) within the diffusion cells, separated from a receptor chamber containing release medium maintained at 37 ± 0.5 °C and stirred at 200 rpm. At predetermined time intervals (1, 2, 3, 4, 5, 6, and 24 h), aliquots were withdrawn from the receptor chamber, replaced with fresh medium, and analyzed for PAC concentration via HPLC-UV at 227 nm [31, 42]. In vitro drug release was calculated using the following equation:

$$\%\ PAC\ Released = \frac{Amount\ of\ PAC\ released\ at\ time\ t}{Total\ amount\ of\ PAC\ in\ the\ formula} x100 \quad (2)$$

Cytotoxicity MTT Assay The KF-28 cell Line was cultured in RPMI 1640 medium supplemented with 10% FBS and 100 µg/mL penicillin/streptomycin, incubated at 37 °C with 5% CO2 to confluence. Cells were seeded at a density of 5000 cells/well in 96-well plates and incubated for 24 h. Subsequently, the medium was replaced with serial dilutions of PAC and BSA-LDH-PAC (10–250 µg/mL) and incubated for 24 h. Following incubation, MTT solution (5 mg/mL) was added for 4 h. Formazan crystals were dissolved with dimethylsulfoxide (DMSO), and absorbance was measured at 570 nm. Cell viability was calculated using the following formula:

$$Cell\ vialbility\ (\%) = \frac{OD - T}{OD - C} \times 100 \quad (3)$$

Where OD-C is the optical density control representing KF-28 cells incubated in medium alone, and OD-T is the optical density of the test specimen representing KF-28 cells treated with the corresponding sample [43]. Statistical analyses were conducted entirely within Microsoft Excel using the Data Analysis Add-in, utilizing Two-way ANOVA to evaluate the effects of treatment group, concentration, and their interaction on cell viability, and Student t-test (for unequal variances) was manually calculated for pairwise comparisons between PAC and BSA-LDH-PAC at each concentration using standard. Results were considered significant at $p<0.05$ [38].

The half-maximal inhibitory concentration (IC_{50}) was determined by fitting the cell viability data to a four-parameter sigmoidal dose-response curve using nonlinear regression. The percentage of cell viability was plotted against the logarithm of drug concentration. The IC_{50} was extracted from the fitted curve as the concentration corresponding to 50% cell viability [38]. Curve fitting was performed using Excel's Solver Add-in to minimize residual errors and estimate model parameters.

FORMAL PARA 10 Stability Studies Plain LDH and BSA-LDH were subjected to stability studies. Samples were prepared by reconstituting LDH and BSA-LDH in phosphate buffer (pH 7.4) at a concentration of 1 mg/mL LDH. Particle size, drug entrapment efficiency, and zeta potential were determined for freshly prepared samples and after storage for 6 months in the refrigerator at 4°C [24].

Results and Discussion

Studying the Effect of Independent Variables on Formulation

The successful application of nanocarriers as drug delivery systems necessitates a comprehensive understanding of their interactions with Biological systems. Key factors influencing nanocarrier uptake and distribution include particle size, surface charge, and surface functionalization. Optimal nanocarrier dimensions facilitate cellular internalization, typically ranging from 50 to 100 nm. Concurrently, a balanced surface charge minimizes non-specific interactions and promotes cellular uptake. Nanocarriers can be further engineered to enhance targeting specificity and drug delivery efficiency by incorporating specific ligands onto their surface. By conjugating proteins, antibodies, or other biomolecules, nanoparticles can be directed at specific cell membrane receptors, increasing intracellular drug concentrations and reducing therapeutic dosages. This study investigates the impact of these parameters on the physicochemical properties and drug delivery potential of LDH-based nanoparticles [7]. Developing efficient drug delivery systems hinges on a comprehensive understanding of nanocarrier characteristics and their interactions with biological environments. This study investigated the impact of key parameters, including particle size, surface charge, and drug loading, on the physicochemical properties and drug delivery potential of LDH-based nanocarriers.

Particle Size

Table 1 summarizes the particle size (PS) values obtained from the fifteen experimental runs (F1-F15). As depicted in Fig. 1A, PAC concentration had negligible effects on LDH particle size.

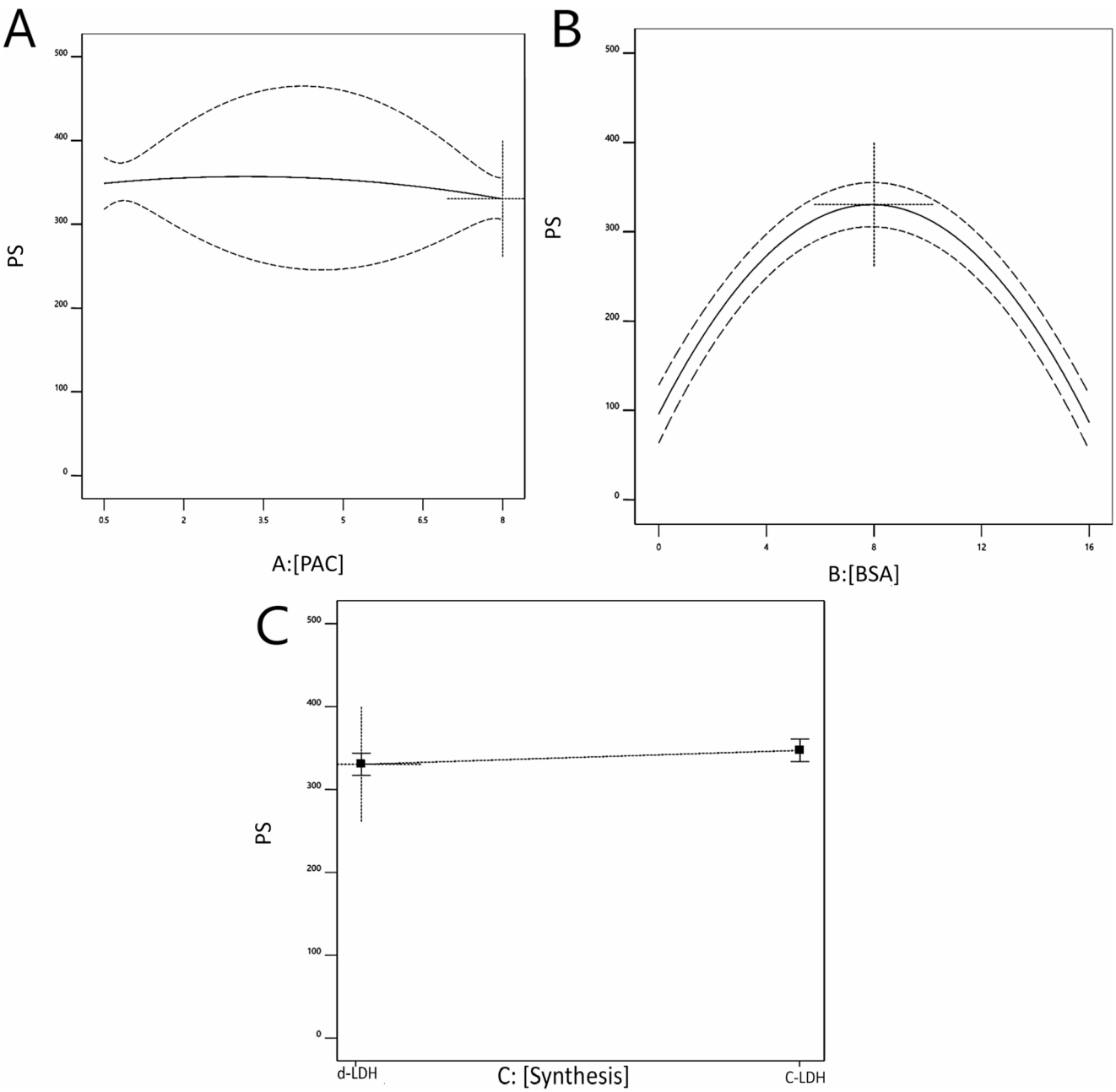

Fig. 1 The effect of (**A**) PAC concentration, (**B**) BSA concentration, and (**C**) post-synthesis treatment on the hydrodynamic diameter of LDH nanoparticles. The solid Lines represent the predicted responses from a D-optimal experimental design, with dashed LInes indicating the 95% confidence intervals. Particle size was measured by dynamic light scattering (DLS). All data points represent the mean ± standard deviation (SD) of three independent experiments ($n = 3$)

In contrast, BSA functionalization, Fig. 1B, significantly influenced particle size ($p < 0.0001$). Increasing BSA concentration led to a gradual increase in particle size, reaching a maximum of 8 mg/mL BSA, followed by a subsequent decrease. BSA functionalization of the optimized formula significantly influenced particle size, leading to an increase at high BSA concentrations and subsequent stabilization at higher levels. BSA-LDH particles produced at high BSA concentrations (16 mg/mL) exhibited an average size of 100 nm, slightly larger than that of d-LDH (89 nm). This suggests effective de-aggregation of BSA-LDH hybrids, enhancing particle stability. The observed size increase is primarily attributed to the formation of a BSA hydrophilic corona around the LDH particles, rather than random aggregation [29]. These findings align with those reported by Gu et al., who demonstrated

that BSA functionalization of LDH particles significantly enhanced their stability in pH 7.4 buffer and water when using a high BSA: LDH ratio (25:2) [29].

The post-synthesis process (Fig. 1C) significantly influenced LDH particle morphology and, consequently, drug loading capacity. Delamination produced nanosheets with increased surface area and accessible interlayer spaces, as evidenced by the TEM micrographs showing smaller, less porous d-LDH-PAC particles than c-LDH-PAC. This structural modification enabled improved drug entrapment. In addition, calcination resulted in larger, porous c-LDH-PAC particles, as observed in TEM images, which, despite potential benefits for drug diffusion, hindered overall drug loading due to partial pore obstruction during reconstruction, as reported by Kim et al. These findings point to the importance of LDH structural integrity in optimizing drug delivery systems, which points to the possibility of delamination as a promising approach for enhancing the performance of LDH-based drug delivery platforms.

Drug Entrapment Efficiency

As shown in Fig. 2A, %EE was highly affected by the formulation variables, with a wide range of %EE from 1.5 ± 0.2% to 51.2 ± 0.5%. In contrast, Fig. 2B illustrates that BSA functionalization minimally influenced PAC entrapment efficiency (%EE). Conversely, drug concentration (Fig. 2A) and post-synthesis treatment (Fig. 2C) significantly impacted ($p < 0.0001$ for both variables) the percentage of entrapped drug. An inverse relationship was observed between drug concentration and EE%, primarily attributed to the saturation of available adsorption sites on LDH particles at higher drug loadings [44]. Additionally, hydrophobic interactions between drug molecules, leading to aggregation, competed with drug-LDH interactions, hindering entrapment within the LDH interlayer spaces [44].

Regarding the post-synthesis treatment described in Sect. 2.2.1, the particles were delaminated using alcohol (d-LDH) and sonication or calcinated via oven treatment (c-LDH). The delamination/calcination process increases the surface area of the particles to increase drug adsorption; hence, the percentage of drug entrapment efficiency is expected to increase. Figure 2C illustrates a significantly higher drug entrapment efficiency for delaminated LDH (d-LDH) than calcined LDH (c-LDH).

The observed high drug loading capacity aligns with the results reported by Mei et al. for monolayered LDH nanosheets (3.6 mg doxorubicin per mg LDH), further supporting the potential of delaminated LDH as a drug delivery platform [45, 46].

Zeta Potential

Figure 3A and C demonstrate negligible changes in particle zeta potential with variations in drug concentration or post-synthesis treatment. In contrast, BSA concentration significantly influenced zeta potential ($p < 0.0001$) as depicted in Fig. 3B.

LDH nanocarriers, characterized by a positive zeta potential of +27 mV, exhibited an initial propensity for cellular uptake due to electrostatic interactions with cancer cell membranes. However, their aggregation in physiological conditions necessitated surface modification. BSA functionalization was the primary determinant of LDH zeta potential, significantly shifting the charge from positive to negative. In contrast, drug concentration and post-synthesis treatment had minimal effects on the zeta potential. Notably, increasing BSA concentration resulted in a more negative zeta potential, which can be associated with improved tumour accumulation for particles of approximately 150 nm [47, 48]. BSA coating enhanced stability, facilitated targeting via Gp60 receptors, and induced a negative zeta potential shift, aligning with BSA's intrinsic charge [47, 48].

Design Validity and Optimization

Formulation variables influencing BSA-LDH-PAC nanocarrier characteristics were optimized using a D-optimal design by minimizing PS and maximizing EE% and ZP. The optimal formulation (F3) was determined using desirability function analysis, yielding a desirability value of 0.993. F3 comprises 16 mg/mL BSA, 0.5 mg/mL PAC, and d-LDH. The freshly formed aqueous dispersion of F3 was subjected to measurements of its particle size, %EE, and zeta potential, resulting in values of 95 ± 0.14 nm, 51 ± 0.54%, and −27 ± 0.1 mV, respectively. The outcomes of the freshly produced sample were contrasted with those ascertained using the D-optimal design. The observed lower magnitude of error (9.8%, 2.7%, and 1.8%) for mean particle size, %EE, and zeta potential, respectively, suggests that there are no significant changes and/or there is a good agreement between the prior and present experimental data. These results demonstrate the robustness of the optimization model in accurately predicting real-world outcomes, as further supported by supplementary data (Table S2) [24].

Physicochemical Characterization of the Optimized Formula F3 (BSA-d-LDH-PAC)

Molecular Modelling and FTIR

As shown in molecular modelling diagram of LDH (Fig. 4A and B), LDH crystals assemble in layers of Mg and Al

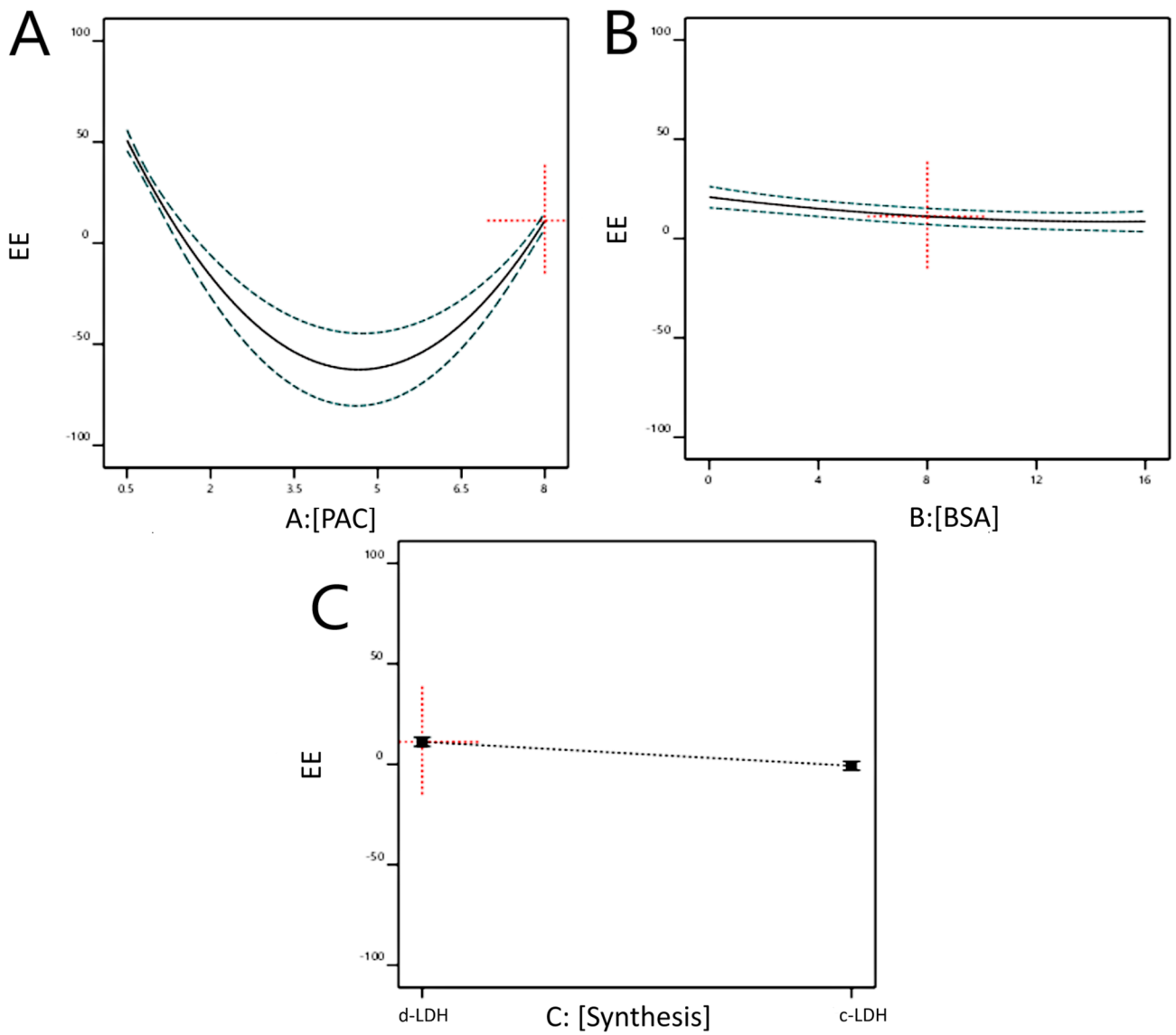

Fig. 2 The effect of (**A**) PAC concentration, (**B**) BSA concentration, and (**C**) post-synthesis treatment on the drug entrapment efficiency (EE) of LDH nanoparticles. The solid Lines represent the predicted responses from a D-optimal experimental design, with dashed LInes indicating the 95% confidence intervals. All data points represent the mean ± standard deviation (SD) of three independent experiments ($n = 3$)

hydroxides bonded together via hydrogen bonding which is confirmed via FTIR (Fig. 5A) of d-LDH showing a very broad band at around 3450 cm − 1 belongs to OH stretching of the hydroxide layer and water with the broadness evident of hydrogen bond formation [49]. The characteristic peaks at 1307 cm − 1 are characteristic of the NO3 − group [50], in addition to strong bands at 290 $cm^{-1}$and 400 cm − 1, whichre attributed to the vibrations of Mg–O and Al–O [51]. The band at about 1009 cm − 1 can be attributed to the deformation vibration of water molecules in the interlayer domain [52]. BSA successfully functionalized LDH functionalization is due to the formation of hydrogen bonds between the OH group in LDH and BSA at multiple sites, which was also confirmed in the IR spectrum of BSA-LDH-PAC, showing characteristic peaks of BSA present in the pure BSA IR spectrum. Moreover, PAC also interacted with both BSA and LDH through hydrogen bonding, resulting in the successful loading of PAC on the surface of LDH [53]. These interactions are evident in BSA-LDH-PAC IR spectrum which retained the characteristic peaks of LDH, BSA and PAC at 2965 cm^{-1} (C–H), 1707 cm − 1 (CO group), 1641 cm^{-1} (C–C stretch), 1370 cm^{-1} (CH3), 1248 cm^{-1} (C–N), 1072 cm^{-1} (C–O) and 709 cm − 1 (C–H off the plane) [53] reflecting the successful strong incorporation of the drug within the particles and accounting for the high percentage of drug entrapped.

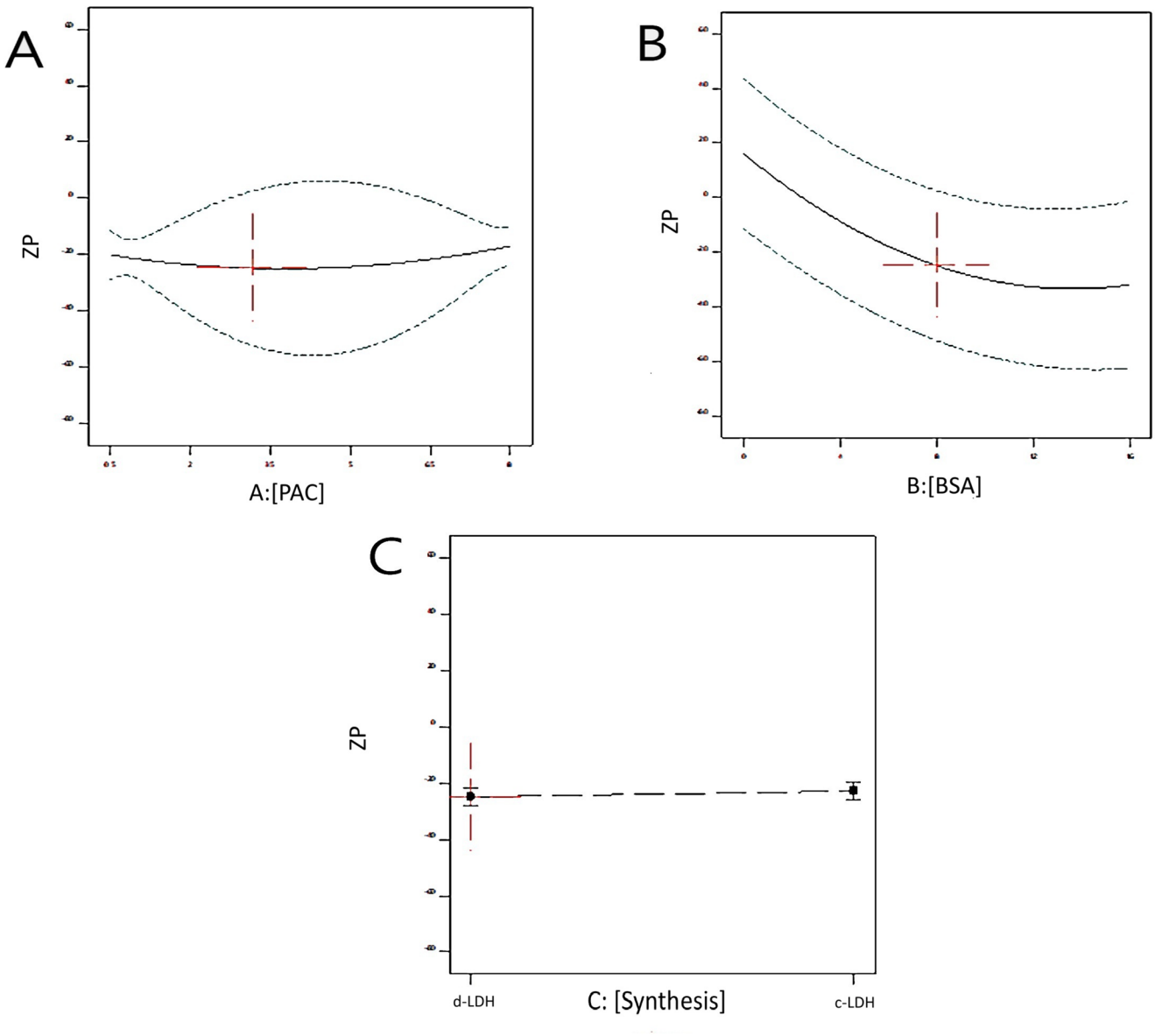

Fig. 3 The effect of (**A**) PAC concentration, (**B**) BSA concentration, and (**C**) post-synthesis treatment on the drug entrapment efficiency (EE) of LDH nanoparticles. The solid Lines represent the predicted responses from a D-optimal experimental design, with the dashed LInes indicating the 95% confidence intervals. All data points represent the mean ± standard deviation (SD) of three independent experiments ($n = 3$)

Transmission Electron Microscopy (TEM)

TEM micrographs (Fig. 6A-B) reveal a brucite-like (hexagonal) morphology for both d-LDH-PAC and c-LDH-PAC particles, consistent with previous reports [29]. However, c-LDH-PAC particles exhibit a larger size compared to d-LDH-PAC, aligning with dynamic light scattering data (Sect. 3.1). Furthermore, c-LDH-PAC displays a porous structure.

Differential Scanning Calorimetry (DSC)

Figure 7 presents the DSC thermograms of pure PAC and the optimized F3 formulation. PAC exhibited a sharp endothermic peak at 218 °C, consistent with the literature [53]. The endothermic peak shifted to 200 °C. The crystalline nature of pure paclitaxel was confirmed by the presence of a sharp endothermic peak at 218 °C in the DSC thermogram, consistent with the literature [53]. In contrast, the broader and less intense endothermic peak observed for the

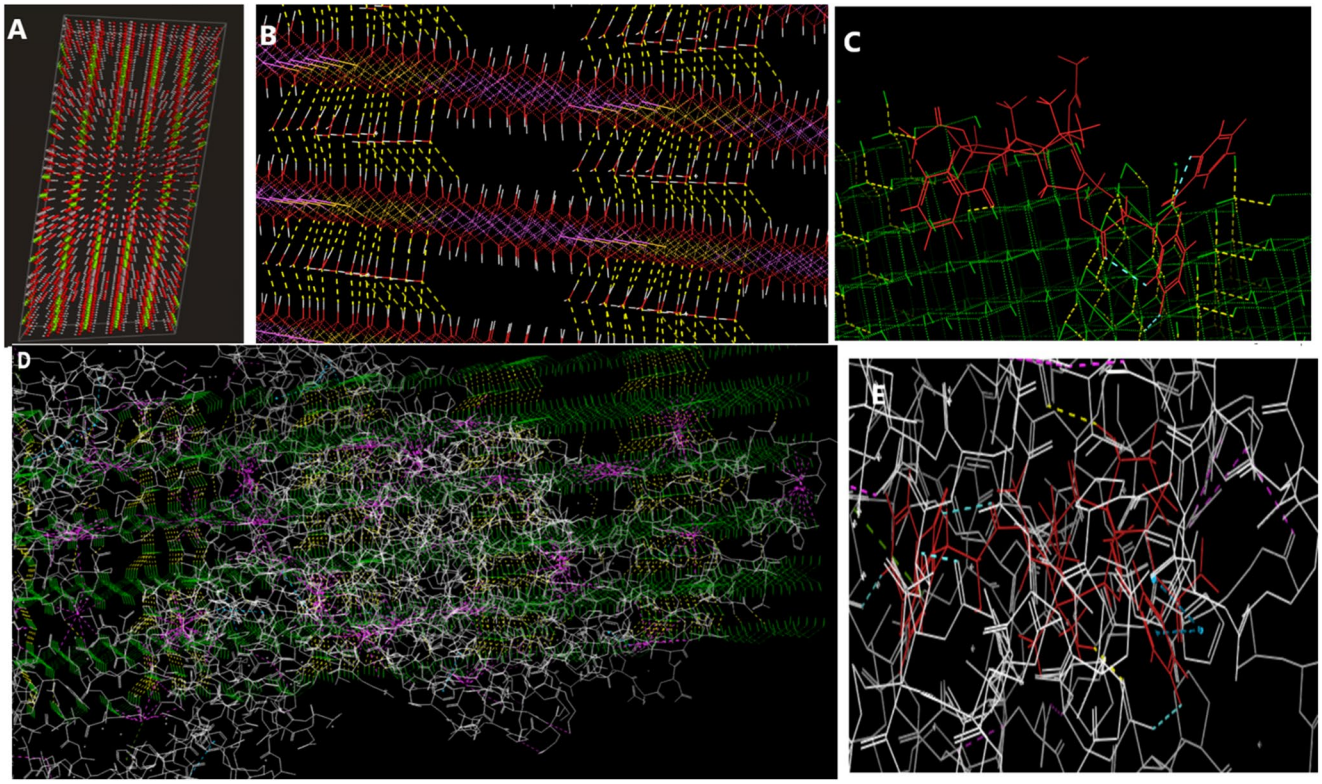

Fig. 4 Molecular modelling data illustrating interactions between different components for (**A**) LDH crystals as acquired from Materials Project and processed using Avogadro Software, (B-D) Molecular modelling data via Maestro software comprising (**B**) LDH layers attached via hydrogen bonds (yellow dotted line), (**C**) Pac molecule (red) and LDH(green) interactions via hydrogen bonds (yellow) and aromatic via hydrogen bonds (cyan blue), (**D**) LDH (green) and albumin (white) interactions via hydrogen bonds (yellow), aromatic hydrogen bonds (cyan blue) and Pi interactions (pink) and (**E**) PAC molecule (red) and albumin (white) interactions via hydrogen bonding (yellow), aromatic hydrogen bonding (cyan blue)

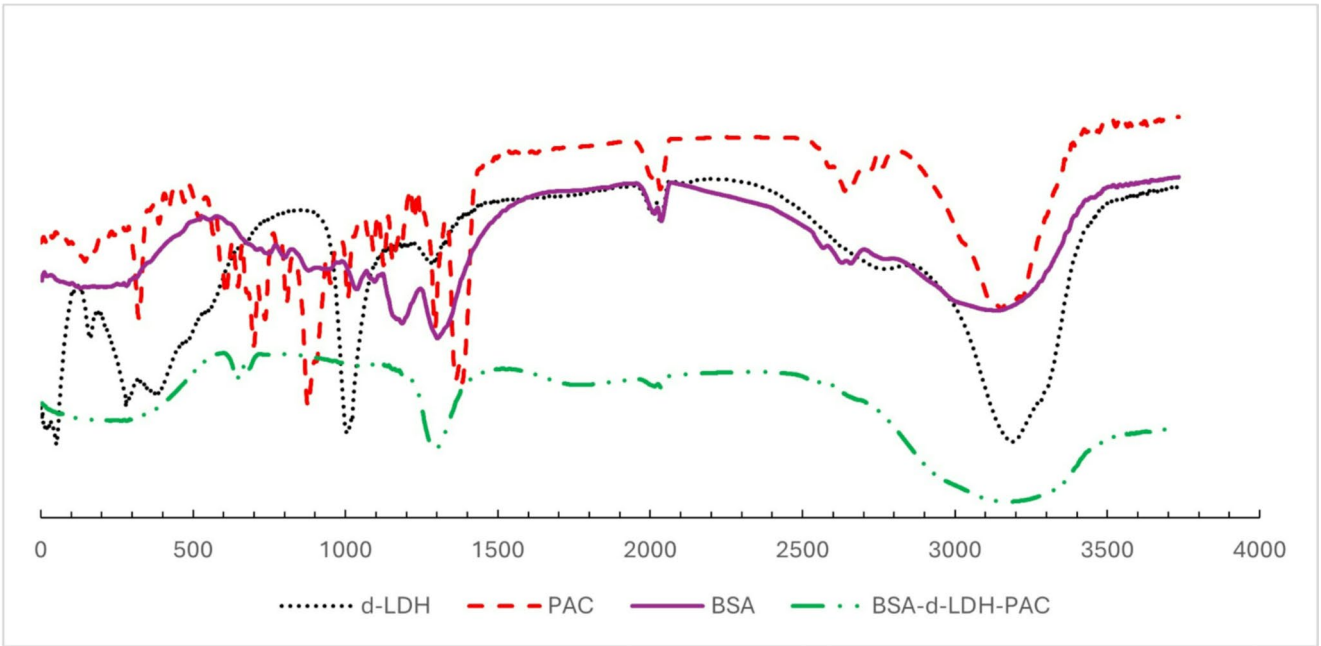

Fig. 5 Fourier-transform infrared (FTIR) spectra of individual components and the final nanocomposite. The graph shows the vibrational spectra of plain d-LDH (dotted black line), PAC (dashed red line), BSA (solid purple line), and the final BSA-d-LDH-PAC nanocomposite (dashed-dotted green line)

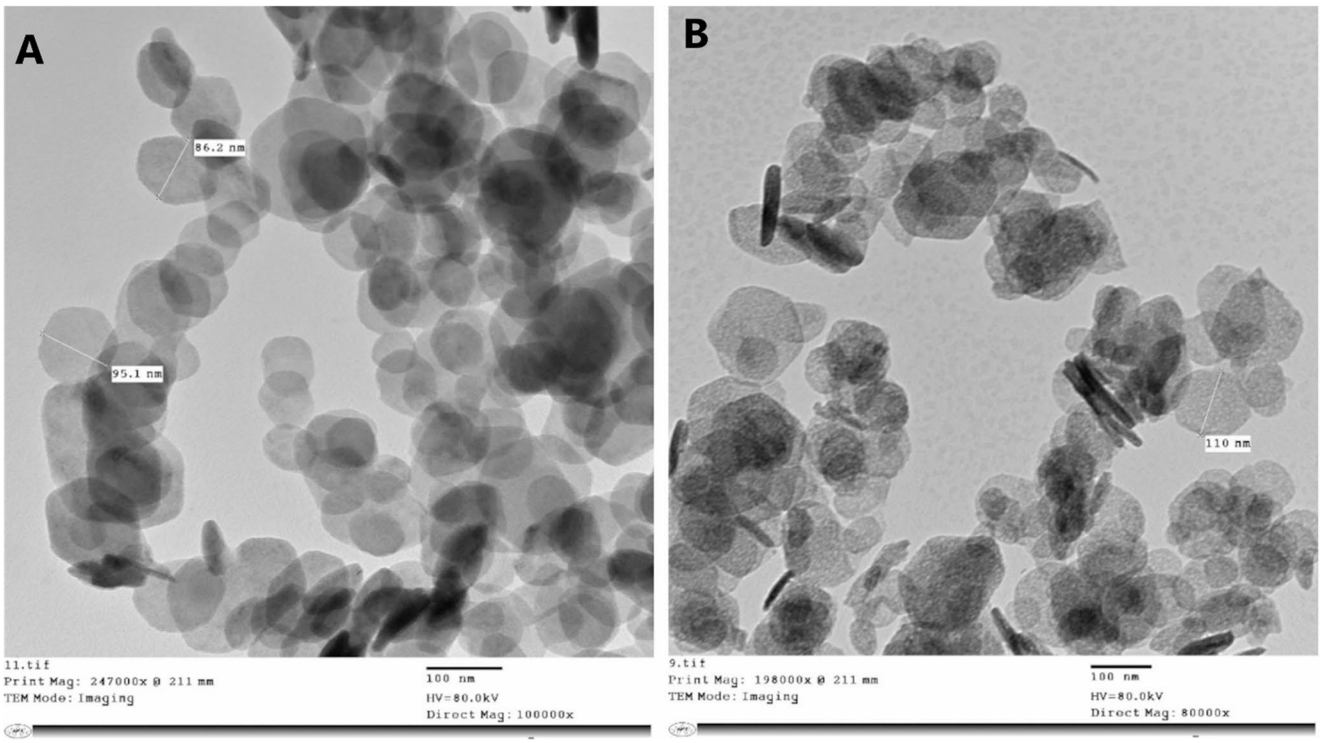

Fig. 6 Transmission electron microscope (TEM) images of (**A**) de-intercalated LDH-PAC (d-LDH-PAC) and (**B**) co-precipitated LDH-PAC (c-LDH-PAC) captured at 80 kV with a 200 nm scale bar

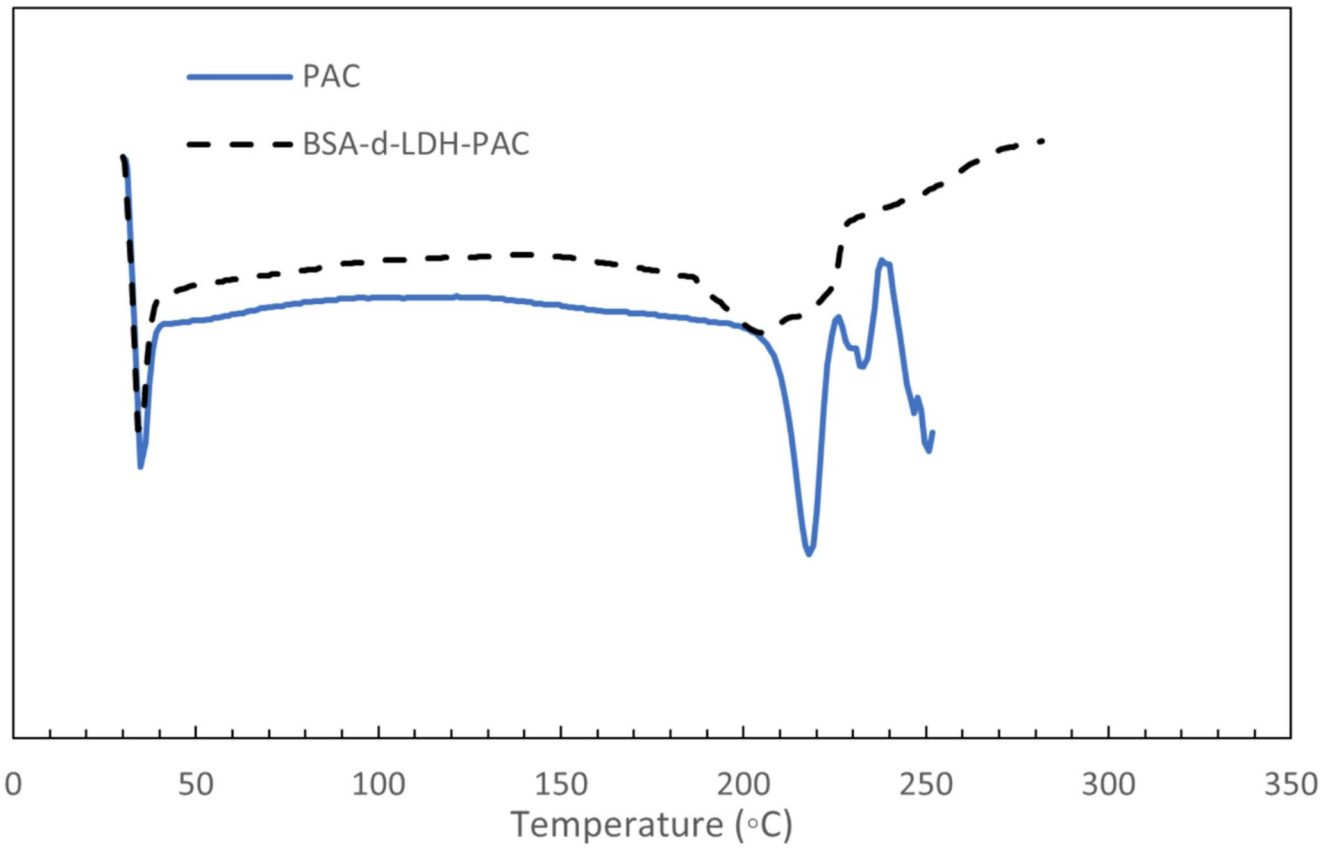

Fig. 7 DSC thermogram of PAC and BSA-d-LDH-PAC

paclitaxel-loaded LDH formulation at 200 °C in the DSC thermogram indicated a reduction in drug crystallinity.

X-ray Diffraction (XRD)

This decrease in crystallinity was further corroborated by the XRD diffractogram (Fig. 8), which compares the XRD diffractograms of pure PAC and PAC incorporated into LDH particles. The diffraction pattern of BSA-d-LDH-PAC exhibits broader and less intense peaks compared to pure PAC, confirming decreased drug crystallinity within LDH particles [39]. The reduced crystallinity of the drug within the LDH particles likely contributed to the enhanced drug solubility and subsequent release profile observed in Sect. 3.3.5 [54, 55].

In Vitro Drug Release

Figure 9 illustrates the pH-dependent release profile of PAC from drug powder and BSA-LDH-PAC formulations. PAC's poor water solubility resulted in negligible release at pH 7.4. LDH exhibited a sustained release pattern at physiological pH, while a pronounced burst release was observed at pH 5.5, with 90% drug release within 5 h [56].

To elucidate the release mechanism of the BSA-LDH-PAC complex, drug release kinetics were fitted to zero-order, first-order, Higuchi, and Korsmeyer-Peppas models. The Korsmeyer-Peppas model exhibited the best fit (R^2 = 0.961 for pH 5.5 and 0.942 for pH 7.4), with a release exponent (n) of 0.4. The pH-responsive behaviour of LDH-based nanocarriers is a key attribute for targeted drug delivery. The observed pH-dependent release profile, with a pronounced burst release at pH 5.5, suggests the potential for effective drug delivery in the acidic tumour microenvironment. This pH-responsive behaviour is attributed to the protonation of LDH surfaces at acidic pH, disrupting drug-LDH interactions and facilitating drug release. Conversely, at higher pH, electrostatic interactions between the drug and LDH inhibit rapid release, leading to a sustained profile. These findings align with previous reports on the pH-dependent drug release behaviour of LDHs [56]. The Korsmeyer-Peppas model suggests a quasi-Fickian diffusion mechanism where the drug diffuses from the LDH interlayer via ion exchange. Notably, the formulation's pH-responsive release behaviour,

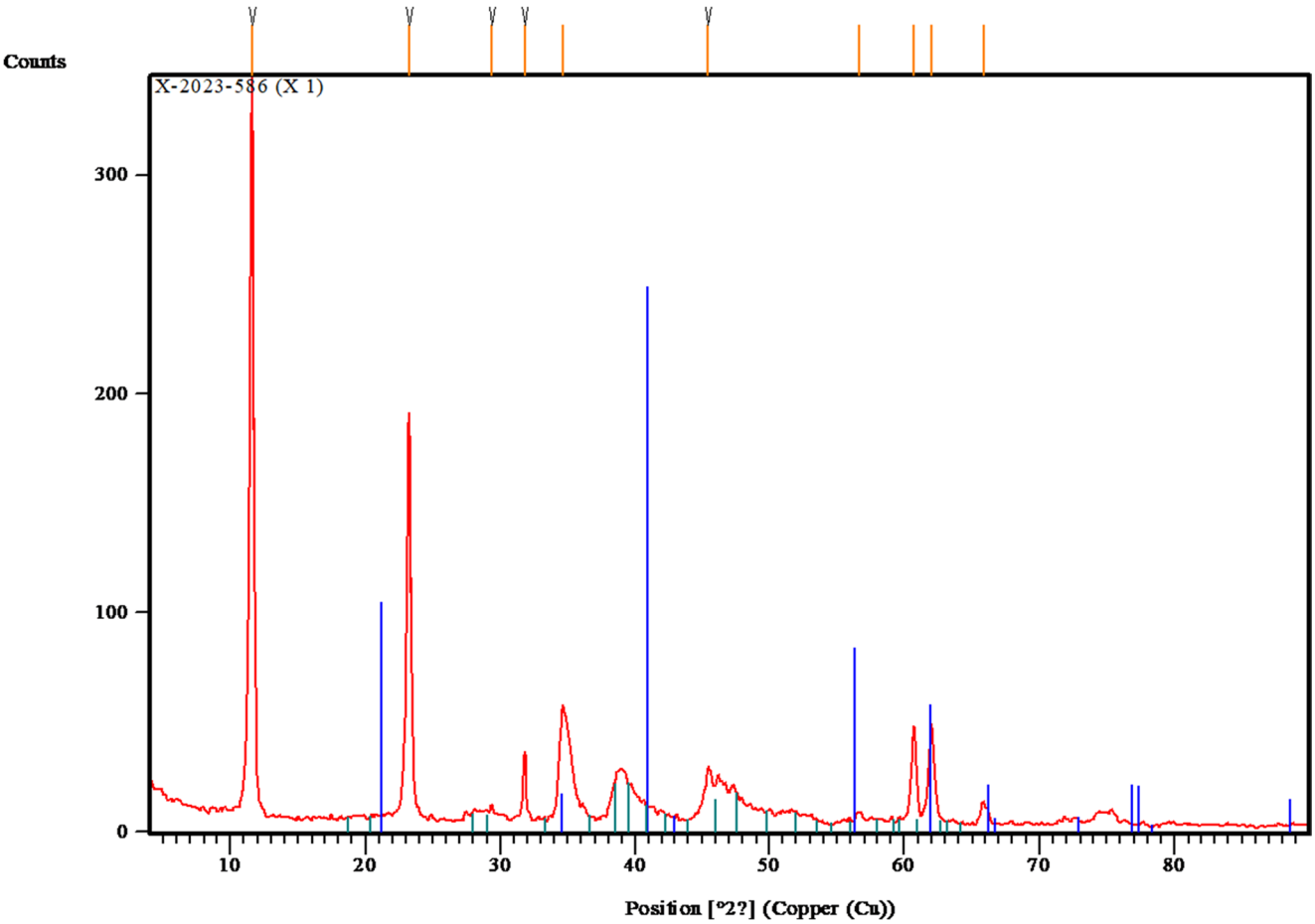

Fig. 8 XRD diffractograms of (blue) PAC and (red) BSA-d-LDH-PAC

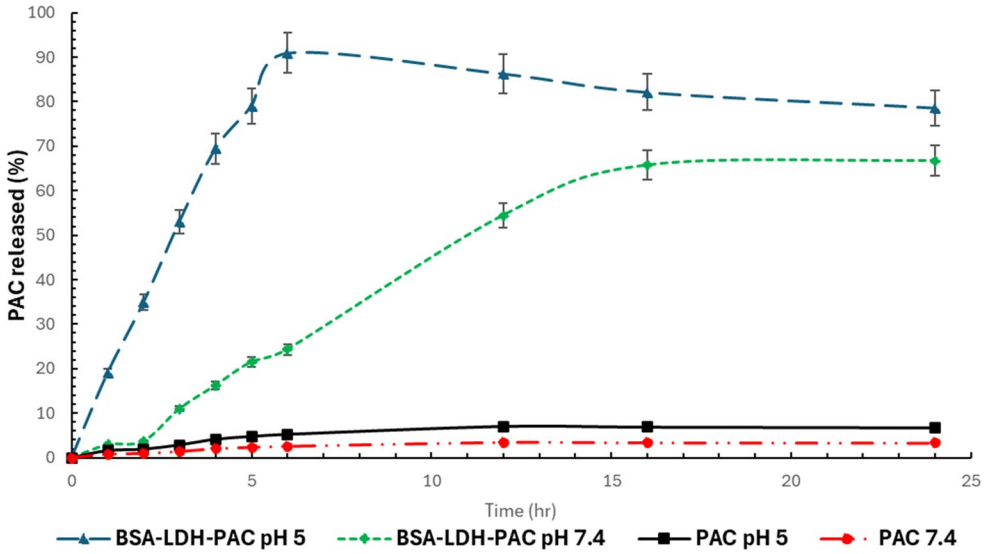

Fig. 9 In vitro drug release profiles of PAC from BSA-LDH-PAC and free PAC at either pH 5.5 or pH 7.4 ($n=6$)

with enhanced drug release in acidic environments, is particularly advantageous for cancer therapy.

Cytotoxicity MTT Assay

Figure 10 depicts the cytotoxic effects of plain LDH, PAC suspension, and BSA-LDH-PAC on KF-28 cells. Plain LDH exhibited negligible cytotoxicity, confirmed by microscopic images as shown in Fig. 11, confirming its suitability as a safe drug carrier, as confirmed by microscopic images in Fig. 11. Free PAC displayed a cytotoxic effect over the range of concentrations from 10 to 250 µg/mL with a calculated IC_{50} of 60.2 µg/mL. Notably, BSA-LDH-PAC displayed a sharper decrease in cytotoxicity compared to PAC, with a considerably lower IC_{50} of 52.7 µg/mL, indicating higher efficacy. Statistical analysis revealed that at lower concentrations (0 and 10 µg/mL), no significant difference was observed between PAC and BSA-LDH-PAC ($p>0.05$). However, starting from 25 µg/mL, BSA-LDH-PAC exhibited significantly lower viability compared to PAC ($p<0.05$). The superior efficacy of BSA-LDH-PAC compared to pure PAC suspension, which is evident in both higher cytotoxic effects and lower IC_{50}, can be attributed to the nanocarriers' ability to be internalized by cells via endocytosis due to their 95 nm size, in addition to their better release profile compared to free PAC [2]. The superior efficacy of BSA-functionalized LDH-entrapped PAC compared to the free drug highlights the potential of this system for overcoming PAC's bioavailability limitations, improving therapeutic outcomes, and reducing systemic side effects. Moreover, BSA-LDH has proven to be a biocompatible, non-toxic carrier due to its low cytotoxicity, which paves the way for its use as a biocompatible drug delivery system. Further studies are warranted to evaluate the in vivo efficacy of this formulation and to explore its applicability to other therapeutic agents.

Stability Studies

Stability studies conducted over six months demonstrated no significant changes ($p>0.05$) in particle size, drug entrapment efficiency, and zeta potential compared to freshly prepared samples (Table 2), indicating satisfactory sample stability.

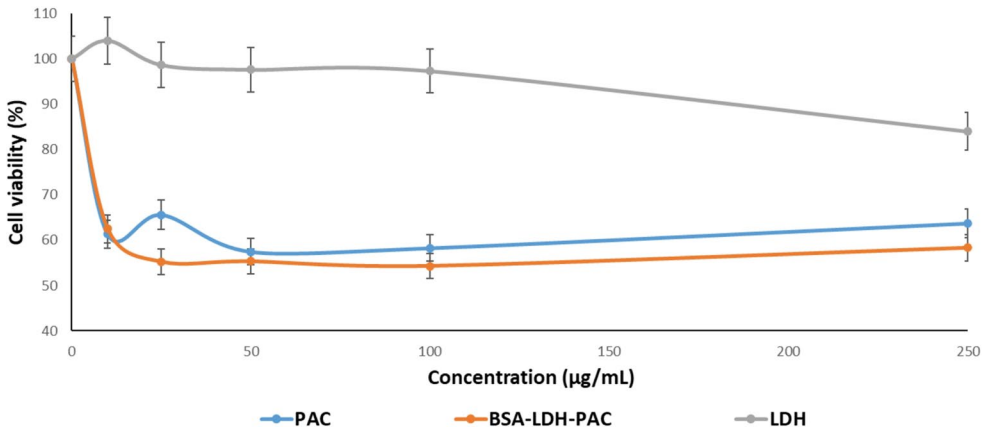

Fig. 10 %Cell viability percentages of KF-28 treated with different concentrations of free PAC, BSA-d-LDH-PAC, and plain BSA-LDH ($n=3$)

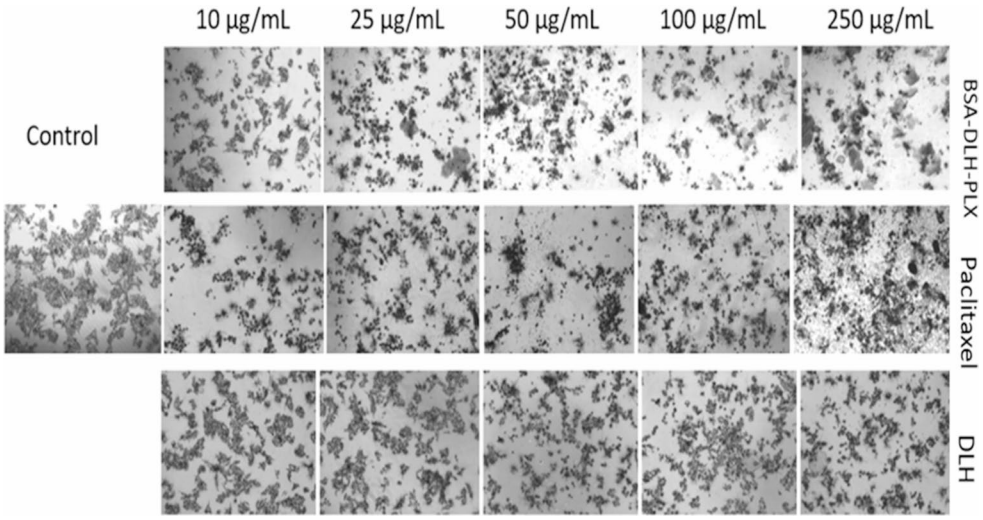

Fig. 11 The microscopic images of KF-28 cells after treatment with the BSA-d-LDH-PAC, PAC, and BSA-d-LDH

Table 2 Stability of the optimized formulation (F3) after 6 months of storage. On the particle size (PS), entrapment efficiency (%EE), and zeta potential (ZP). Data are presented as the mean ± standard deviation from three independent experiments ($n = 3$)

Parameter	Freshly prepared sample	Stored sample after six months
PS (nm)	95.2 ± 0.14	97.1 ± 1.05
EE%	51.2 ± 0.54	51.5 ± 1.83
Zp (mv)	−27.1 ± 0.1	−26.7 ± 0.1

Chemotherapy, exemplified by paclitaxel (PAC), often induces severe systemic side effects due to indiscriminate drug distribution. To address this, a targeted drug delivery system utilizing layered double hydroxide (LDH) nanocarriers was developed. The developed BSA-functionalized LDH nanocarriers offer a promising platform for paclitaxel delivery. PAC was successfully loaded onto delaminated LDH (d-LDH) and subsequently stabilized with bovine serum albumin (BSA) to enhance stability, facilitate cellular uptake, and improve drug targeting via the GP60 pathway. Optimization of formulation parameters using D-optimal design led to the identification of an optimal formulation (F3) characterized by desirable properties including particle size (95 nm), drug entrapment efficiency (51%), and zeta potential (−27 mV). These results validate the stability of the formulation after six months, which would be beneficial in its translation from the lab to industrial applications. However, further studies under accelerated and long-term conditions, including hot temperature, humidity, and light exposure, are warranted to fully establish the long-term robustness and translational potential of the formulation.

Conclusion

This study presents a promising strategy to improve the delivery and effectiveness of paclitaxel (PAC), a widely used but highly toxic chemotherapeutic agent. By combining delaminated layered double hydroxide (d-LDH) with bovine serum albumin (BSA), we created a smart, targeted nanocarrier that not only stabilizes the drug but also enhances its accumulation in ovarian cancer tissues. The formulation showed excellent long-term stability, selective drug release in acidic environments typical of tumor sites, and significantly improved cytotoxicity against ovarian cancer cells compared to the free drug. These findings highlight the novelty and potential of BSA-d-LDH-PAC as a more efficient and safer alternative to conventional PAC therapy. With further validation in animal models and clinical settings, this approach could pave the way for more targeted and patient-friendly cancer treatments.

Supplementary Information The online version contains supplementary material available at https://doi.org/10.1007/s12247-025-10104-6.

Acknowledgements The authors would like to acknowledge the efforts of Bachelor of Pharmacy students Mr. Omar Maher, Mr. Bashar Farag, and Ms. Hagar Elshirbiny in some of the characterizations in this manuscript during their graduation project in the Faculty of Pharmacy, October for Modern Sciences and Arts University (MSA).

Author Contributions The authors would like to acknowledge the efforts of Bachelor of Pharmacy students Mr. Omar Maher, Mr. Bashar Farag, and Ms. Hagar Elshirbiny in some of the characterizations in this manuscript during their graduation project in the Faculty of Pharmacy, October for Modern Sciences and Arts University (MSA).

Funding Open access funding provided by The Science, Technology & Innovation Funding Authority (STDF) in cooperation with The Egyptian Knowledge Bank (EKB). The authors declare that no funds, grants, or other support were received during the preparation of this manuscript.

Data Availability The authors confirm that the data supporting this study's findings are available within the article. The corresponding author can share the data upon reasonable request.

Declarations

Ethical Statement The MSA research and ethics committee approved all the procedures conducted in this study (application number PT7/Ec7/2022F).

Declaration of generative AI in scientific writing During the preparation of this work, the author(s) used ChatGPT 3.5 to improve the readability and language of the manuscript. After using this tool/service, the author(s) reviewed and edited the content as needed and take full responsibility for the content of the published article.

Competing interests The authors declare no competing interests.

References

1. Webb PM, Jordan SJ. Global epidemiology of epithelial ovarian cancer. Nat Rev Clin Oncol. 2024;21:389–400.
2. Senapati S, Thakur R, Verma SP, Duggal S, Mishra DP, Das P, et al. Layered double hydroxides as an effective carrier for anticancer drugs and tailoring of release rate through interlayer anions. J Controlled Release. 2016;224:186–98.
3. Zhu Y, Wang L, Li Y, Huang Z, Luo S, He Y, et al. Injectable pH and redox dual-responsive hydrogels based on self-assembled peptides for anti-tumor drug delivery. Biomater Sci. 2020;8:5415–26.
4. Raza F, Zhu Y, Chen L, You X, Zhang J, Khan A, et al. Paclitaxel-loaded pH-responsive hydrogel based on self-assembled peptides for tumor targeting. Biomater Sci. 2019;7:2023–36.
5. Raza F, Zafar H, Zhu Y, Ren Y, -Ullah A, Khan A, et al. A review on recent advances in stabilizing peptides/proteins upon fabrication in hydrogels from biodegradable polymers. Pharmaceutics. 2018;10:16.
6. Baird RD, Tan DSP, Kaye SB. Weekly paclitaxel in the treatment of recurrent ovarian cancer. Nat Rev Clin Oncol. 2010;7:575–82.
7. Raza F, Zafar H, Khan MW, Ullah A, Khan AU, Baseer A, et al. Recent progress has been made in the targeted delivery of Paclitaxel nanomedicine for cancer therapy. Mater Adv. 2022;3:2268–90.
8. Jordan MA, Wilson L. Microtubules as a target for anticancer drugs. Nat Rev Cancer. 2004;4:253–65.
9. Spada A, Emami J, Sanaee F, Aminpour M, Paiva IM, Tuszynski J, et al. Design and evaluation of albumin nanoparticles for the delivery of a novel β-tubulin polymerization inhibitor. J Pharm Pharm Sci. 2021;24:344–62.
10. Gallego-Jara J, Lozano-Terol G, Sola-Martínez RA, de Cánovas-Díaz M. Diego Puente T. A compressive review about Taxol®: history and future challenges. Molecules. 2020;25:5986.
11. Lu J, Liong M, Zink JI, Tamanoi F. Mesoporous silica nanoparticles as a delivery system for hydrophobic anticancer drugs. Small. 2007;3:1341–6.
12. Yu S, Gao X, Baigude H, Hai X, Zhang R, Gao X, et al. Inorganic nanovehicle for potential targeted drug delivery to tumor cells, tumor optical imaging. ACS Appl Mater Interfaces. 2015;7:5089–96.
13. Tagaya H, Sato S, Morioka H, Kadokawa J, Karasu M, Chiba K. Preferential intercalation of isomers of naphthalenecarboxylate ions into the interlayer of layered double hydroxides. Chem Mater. 1993;5:1431–3.
14. Gasser MS. Inorganic layered double hydroxides as ascorbic acid (vitamin C) delivery system—intercalation and their controlled release properties. Colloids Surf B Biointerfaces. 2009;73:103–9.
15. Aisawa S, Sasaki S, Takahashi S, Hirahara H, Nakayama H, Narita E. Intercalation of amino acids and oligopeptides into Zn–Al layered double hydroxide by coprecipitation reaction. J Phys Chem Solids. 2006;67:920–5.
16. Nakayama H, Wada N, Tsuhako M. Intercalation of amino acids and peptides into Mg–Al layered double hydroxide by reconstruction method. Int J Pharm. 2004;269:469–78.
17. Choy J-H, Kwak S-Y, Park J-S, Jeong Y-J, Portier J. Intercalative nanohybrids of nucleoside monophosphates and DNA in layered metal hydroxide. J Am Chem Soc. 1999;121:1399–400.
18. Chen M, Cooper HM, Zhou JZ, Bartlett PF, Xu ZP. Reduction in the size of layered double hydroxide nanoparticles enhances the efficiency of SiRNA delivery. J Colloid Interface Sci. 2013;390:275–81.
19. Ladewig K, Niebert M, Xu ZP, Gray PP, Lu GQM. Efficient siRNA delivery to mammalian cells using layered double hydroxide nanoparticles. Biomaterials. 2010;31:1821–9.
20. Khan AI, Lei L, Norquist AJ. Oâ€™Hare D. Intercalation and controlled release of pharmaceutically active compounds from a layered double hydroxideelectronic supplementary information (ESI) available: fig. S1: X-ray diffraction patterns of (a) [LiAl2(OH)6]Cl·H2O and (b) ldh/ibuprofen intercalate. Chem Commun. 2001;2342–3.
21. LI B, HE J, DUAN GEVANSD. Inorganic layered double hydroxides as a drug delivery system?intercalation and in vitro release of Fenbufen. Appl Clay Sci. 2004;27:199–207.
22. Hakeem A, Zhan G, Xu Q, Yong T, Yang X, Gan L. Facile synthesis of pH-responsive doxorubicin-loaded layered double hydroxide for efficient cancer therapy. J Mater Chem B. 2018;6:5768–74.
23. Vajedi FS, Dehghani H, Zarrabi A. Design and characterization of a novel pH-sensitive biocompatible and multifunctional nanocarrier for in vitro Paclitaxel release. Materials Science and Engineering: C. 2021;119:111627.
24. Ibrahim MS, Elkady OA, Amer MA, Noshi SH. Exploiting response surface D-optimal design study for preparation and optimization of spanlastics loaded with miconazole nitrate as a model antifungal drug for topical application. J Pharm Innov. 2023;18:2402–18.
25. Peralta MF, Mendieta SN, Scolari IR, Granero GE, Crivello ME. Synthesis and release behavior of layered double hydroxides–carbamazepine composites. Sci Rep. 2021. https://doi.org/10.1038/s41598-021-00117-9.

26. Oh J-M, Choi S-J, Lee G-E, Han S-H, Choy J-H. Inorganic Drug-Delivery nanovehicle conjugated with Cancer-Cell-Specific ligand. Adv Funct Mater. 2009;19:1617–24.
27. Huang Z, Wang N, Li X, An QF. Calcination of layered double hydroxide membrane with enhanced nanofiltration performance. J Ind Eng Chem. 2020;89:368–74.
28. Choy JH, Oh JM, Choi SJ. 4.37 Layered Double Hydroxides as Controlled Release Materials. Comprehensive Biomaterials II. Elsevier; 2017. pp. 705–18.
29. Gu Z, Zuo H, Li L, Wu A, Xu ZP. Pre-coating layered double hydroxide nanoparticles with albumin to improve colloidal stability and cellular uptake. J Mater Chem B. 2015;3:3331–9.
30. Griffiths PC, Cattoz B, Ibrahim MS, Anuonye JC. Probing the interaction of nanoparticles with mucin for drug delivery applications using dynamic light scattering. Eur J Pharm Biopharm. 2015;97:218–22.
31. Noshi SH, Ibrahim MS, Salama A, Fathy IA, Elsayyad NME. Chondroitin Sulphate-Chitosan polyelectrolyte complexes for etorocoxib transdermal delivery: in silico, in vitro and in vivo studies. Pharm Dev Technol. 2023;1–19.
32. Danhier F, Lecouturier N, Vroman B, Jérôme C, Marchand-Brynaert J, Feron O, et al. Paclitaxel-loaded pegylated PLGA-based nanoparticles: in vitro and in vivo evaluation. J Controlled Release. 2009;133:11–7.
33. Elsayyad NME, Gomaa I, Salem MA, Amer R, El-Laithy HM. Efficient lung-targeted delivery of risedronate sodium/vitamin D3 conjugated PAMAM-G5 dendrimers for managing osteoporosis: pharmacodynamics, molecular pathways and metabolomics considerations. Life Sci. 2022;309:121001.
34. Nosrati H, Abbasi R, Charmi J, Rakhshbahar A, Aliakbarzadeh F, Danafar H, et al. Folic acid conjugated bovine serum albumin: an efficient smart and tumor targeted biomacromolecule for inhibition folate receptor positive cancer cells. Int J Biol Macromol. 2018;117:1125–32.
35. IBRAHIM MS, ELMAHDY ELSAYYAD NM SALAMAA, NOSHI SH, QUALITY BY DESIGN (QBD) AS A TOOL FOR THE OPTIMIZATION OF INDOMETHACIN FREEZE-DRIED SUBLINGUAL TABLETS. : IN VITRO AND IN VIVO EVALUATION. Int J Appl Pharm. 2021;160–71.
36. Hanwell MD, Curtis DE, Lonie DC, Vandermeersch T, Zurek E, Hutchison GR. Avogadro: an advanced semantic chemical editor, visualization, and analysis platform. J Cheminform. 2012;4:17.
37. Elsayyad NME, Salama A, Noshi SH. Concurrent tissue engineering and infection prophylaxis utilising stable dual action amoxicillin loaded scaffolds. J Drug Deliv Sci Technol. 2020;58:101788.
38. Elsayyad NME, Ibrahim MS, Noshi SH. Sustainable pH-responsive casein/hyaluronic acid layered nanoparticles for targeted delivery of Metformin to colorectal cancer. J Drug Deliv Sci Technol. 2025. https://doi.org/10.1016/j.jddst.2025.106710.
39. Ibrahim MS, Elsayyad NME, Salama A, Noshi SH. Utilization of response surface design for development and optimization of Rosuvastatin calcium loaded nano-squarticles for hair growth stimulating VEGF and IGF production: In-vitro and in-vivo evaluation. Drug Dev Ind Pharm. 2023;1–14.
40. Noshi H, Basha S, Awad MEA, Mohamed Elmahdy Elsayyad G. N. Miconazole Nitrate loaded Soluplus®-Pluronic® nano-micelles as promising Drug Delivery Systems for Ocular Fungal Infections: In vitro and In vivo Considerations. Res J Pharm Technol. 2022;501–11.
41. El-Maraghy CM, Saleh SS, Ibrahim MS, El-Naem OA. Green wastewater treatment of repurposed COVID-19 therapy (levofloxacin) using synthesized magnetite pectin nanoparticles, comparison with mesoporous silica nanoparticles. BMC Chem. 2023;17:134.
42. Ge F, Qiao R, Song P, Tao Y, Zhu L, Zhang W, et al. Construction of the targeted and pH-sensitive Paclitaxel drug delivery system RGD/PTX@ZIF-90 and anti-tumor activity research. Mater Res Express. 2021;8:045012.
43. Kuittinen T, Rovio P, Luukkaala T, Laurila M, Grénman S, Kallioniemi A, et al. Paclitaxel, carboplatin and 1,25-D3 inhibit proliferation of ovarian cancer cells *in vitro*. Anticancer Res. 2020;40:3129–38.
44. Jaradat A, Obeidat WM. Investigating the correlation between drug physical properties and physical characteristics and drug entrapment efficiencies of Chitosan-TPP nanoparticles. J Pharm Sci. 2023;112:3185–96.
45. Kameda T, Ikeda D, Kumagai S, Saito Y, Yoshioka T. Synthesis of layered double hydroxide nanosheets in an aqueous solvent and their Ni2+ uptake characteristics. Appl Clay Sci. 2021;200:105911.
46. Mei X, Xu S, Hu T, Peng L, Gao R, Liang R, et al. Layered double hydroxide monolayers for controlled loading and targeted delivery of anticancer drugs. Nano Res. 2018;11:195–205.
47. Li R, Wu Z, Wangb Y, Ding L, Wang Y. Role of pH-induced structural change in protein aggregation in foam fractionation of bovine serum albumin. Biotechnol Rep. 2016;9:46–52.
48. Németh Z, Csóka I, Semnani Jazani R, Sipos B, Haspel H, Kozma G, et al. Quality by design-driven zeta potential optimisation study of liposomes with charge imparting membrane additives. Pharmaceutics. 2022;14:1798.
49. Benhiti R, Ait Ichou A, Zaghloul A, Carja G, Zerbet M, Sinan F, et al. Kinetic, isotherm, thermodynamic and mechanism investigations of dihydrogen phosphate removal by MgAl-LDH. Nanotechnology for Environmental Engineering. Springer Science and Business Media Deutschland GmbH; 2021.
50. Shabanian M, Hajibeygi M, Raeisi A. FTIR characterization of layered double hydroxides and modified layered double hydroxides. 2020; Available from: https://doi.org/10.1016/B978-0-08-101903-0.00002-1
51. Demeester A, Douma F, Cousin R, Siffert S, Pourceau G, Wadouachi A, et al. Carboxymethyl β-cyclodextrin assistance for the 4-nitrophenol reduction using Cobalt-based layered double hydroxides. Int J Mol Sci. 2024. https://doi.org/10.3390/ijms25126390.
52. Novell Leruth G, Kuznetsova A, Tedim J, Gomes JRB, Galvão TLP. Molecular dynamics model to explore the initial stages of anion exchange involving layered double hydroxide particles. Nanomaterials. 2022;12:4039.
53. Martins KF, Messias AD, Leite FL, Duek EAR. Preparation and characterization of paclitaxel-loaded PLDLA microspheres. Mater Res. 2014;17:650–6.
54. Qin L, Wang M, Zhu R, You S, Zhou P, Wang S. The in vitro sustained release profile and antitumor effect of etoposide-layered double hydroxide nanohybrids. Int J Nanomed. 2013;8:2053–64.
55. Jung SY, Kim HM, Hwang S, Jeung DG, Rhee KJ, Oh JM. Physicochemical properties and hematocompatibility of layered double hydroxide-based anticancer drug methotrexate delivery system. Pharmaceutics. 2020;12:1–14.
56. Bi X, Zhang H, Dou L. Layered double hydroxide-based nanocarriers for drug delivery. Pharmaceutics. 2014;6:298–332.